

Is shrub expansion into grasslands pushed or pulled? A
spatial integral projection model for woody plant
encroachment

Trevor Drees^{*a,b}, Brad M. Ochocki^b, Scott L. Collins^c, and Tom E.X. Miller^b

^aDepartment of Biology, Penn State University, State College, PA USA

^bProgram in Ecology and Evolutionary Biology, Department of BioSciences, Rice
University, Houston, TX USA

^cDepartment of Biology, University of New Mexico, Albuquerque, NM USA

June 29, 2022

^{*}thd5066@psu.edu

1 Abstract

2 **Encroachment**¹ of shrubs into adjacent grasslands has become an increasingly reported
3 phenomenon across the world, and such encroachment is either pulled forward by high
4 population growth at the low-density encroachment front or pushed forward by higher-
5 density areas behind the front. However, at sites such as Sevilleta National Wildlife
6 Refuge in central New Mexico, little is known about whether encroachment is pushed or
7 pulled, and the dynamics of encroachment are not well-understood. Here, long-term en-
8 croachment of creosotebush (*Larrea tridentata*), a native perennial shrub, stands in stark
9 contrast with the stagnation in encroachment observed in recent decades. In order to
10 better understand creosotebush encroachment at this site, we quantify it using a spatially
11 structured population model where a wave of individuals travels at a speed governed by
12 both dispersal and density-dependence. Results indicate that population growth rates
13 generally increase with decreasing density, suggesting that encroachment is pulled by
14 individuals at the low-density wave front, and the spatial population model predicts an
15 encroachment rate of less than 2 cm per year. While the predicted rate of encroach-
16 ment is consistent with observations over recent decades, it does not explain long-term
17 creosotebush encroachment at the study site, suggesting that this process may occur in
18 pulses when recruitment, seedling survival, or dispersal significantly exceed typical rates.
19 Overall, our work demonstrates that individuals at low densities are likely the biggest
20 contributors to creosotebush encroachment at this site, and that this encroachment is
21 likely a process that occurs in large but infrequent bursts rather than at a steady pace.

22 Keywords

23 density-dependence, ecotones, woody encroachment, shrubs, integral projection model,
24 grassland

¹*I am not editing the abstract for now.*

25 Introduction

26 The recent and ongoing encroachment of shrubs and other woody plants into adjacent
27 grasslands has caused significant vegetation changes across arid and semi-arid landscapes
28 worldwide (Van Auken, 2000, 2009; Goslee et al., 2003; Gibbens et al., 2005; Parizek et al.,
29 2002; Cabral et al., 2003; Trollope et al., 1989; Roques et al., 2001). The process of en-
30 croachment generally involves increases in the number or density of woody plants in both
31 time and space (Van Auken, 2000), which can drive shifts in plant community structure
32 and alter ecosystem processes (Schlesinger et al., 1990; Ravi et al., 2009; Schlesinger
33 and Pilmanis, 1998; Knapp et al., 2008). Other effects of encroachment include changes
34 in ecosystem services (Reed et al., 2015; Kelleway et al., 2017), declines in biodiversity
35 (Ratajczak et al., 2012; Sirami and Monadjem, 2012; Brandt et al., 2013), and economic
36 losses in areas where the proliferation of shrubs adversely affects grazing land and pastoral
37 production (Mugasi et al., 2000; Oba et al., 2000).

38 Woody plant encroachment can be studied through the lens of spatial population
39 biology as a wave of individuals that may expand across space and over time (Kot et al.,
40 1996; Neubert and Caswell, 2000; Wang et al., 2002; Pan and Lin, 2012). Theory pre-
41 dicts that the speed of wave expansion depends on two processes: local demography and
42 dispersal of propagules. First, local demographic processes include recruitment, survival,
43 growth, and reproduction, which collectively determine the rate at which newly colonized
44 locations increase in density and produce new propagules. Second, colonization events
45 are driven by the spatial dispersal of propagules, which is commonly summarized as a
46 probability distribution of dispersal distance, or “dispersal kernel”. The speed at which
47 expansion waves move is highly dependent upon the shape of the dispersal kernel, espe-
48 cially long-distance dispersal events in the tail of the distribution (Skarpaas and Shea,
49 2007). Both demography and dispersal may depend on plant size, since larger plants
50 often have improved demographic performance and release seeds from greater heights,

51 leading to longer dispersal distances (Nathan et al., 2011). Accounting for population
52 structure, including size structure, may therefore be important for understanding and
53 predicting wave expansion dynamics (Neubert and Caswell, 2000).

54 Theory predicts that the nature of conspecific density dependence is another critical
55 feature of expansion dynamics but this is rarely studied in the context of woody plant
56 encroachment. Expansion waves typically correspond to gradients of conspecific density
57 – high in the back and low at the front – and demographic rates may be sensitive to
58 density due to intraspecific interactions like competition or facilitation. If the demo-
59 graphic effects of density are strictly negative due to competitive effects that increase
60 with density then demographic performance is maximized as density goes to zero, at the
61 leading edge of the wave. Under these conditions, the wave is “pulled” forward by indi-
62 viduals at the low-density vanguard (Kot et al., 1996), and targeting these individuals
63 and locations would be the most effective way to slow down or prevent encroachment
64 (cite?). However, woody encroachment systems often involve positive feedbacks whereby
65 shrub establishment modifies the environment in ways that facilitate further shrub re-
66 cruitment. For example, woody plants can modify their micro-climates in ways that
67 elevate nighttime minimum temperatures, promoting conspecific recruitment and sur-
68 vival for freeze-sensitive species (D’Odorico et al., 2010; Huang et al., 2020). Positive
69 density dependence (or Allee effects) causes demographic rates to be maximized at higher
70 densities behind the leading edge, which “push” the expansion forward, leading to qualita-
71 tively different expansion dynamics (Kot et al., 1996; Taylor and Hastings, 2005; Sullivan
72 et al., 2017; Lewis and Kareiva, 1993; Veit and Lewis, 1996; Keitt et al., 2001). Pushed
73 expansion waves generally have different shapes (steeper density gradients) and slower
74 speeds than pulled waves (Gandhi et al., 2016), and may require different strategies for
75 managing or decelerating expansion (check Taylor and Hastings ref). The potential for
76 positive feedbacks is well documented in woody encroachment systems but it remains un-
77 clear whether and how strongly these feedbacks decelerate shrub expansion and influence

78 strategies for management of woody encroachment.

79 In this study, we linked woody plant encroachment to ecological theory for invasion
80 waves, with the goals of understanding how seed dispersal and density-dependent demog-
81 raphy drive encroachment, and determining whether the encroachment wave is pushed or
82 pulled. Throughout the aridlands of the southwestern United States, shrub encroachment
83 into grasslands is well documented (D’Odorico et al., 2012) but little is known about the
84 dispersal and demographic processes that govern it. Our work focused on encroachment
85 of creosotebush (*Larrea tridentata*) in the northern Chihuahuan Desert. Expansion of
86 this species into grasslands over the past 150 years has been well documented, leading to
87 decreased cover of *Bouteloua eriopoda*, the dominant foundation species of Chihuahuan
88 desert grassland (Gardner, 1951; Buffington and Herbel, 1965; Gibbens et al., 2005).
89 As in many woody encroachment systems, creosotebush expansion generates ecotones
90 marking a transition from dense shrubland to open grassland, with a transition zone in
91 between where shrubs can often be found interspersed among grasses (Fig. 1).

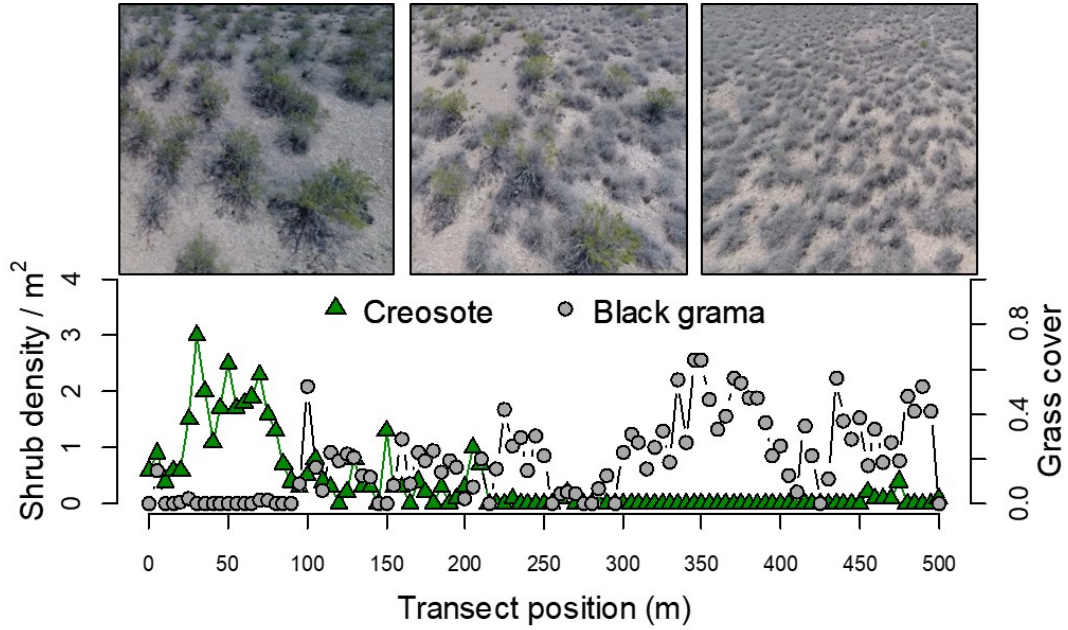


Figure 1: Example of an ecotone transect at Sevilleta LTER, spanning gradients of creosotebush and black grama grass. Photo credits: TEX Miller

Historically, creosotebush encroachment into grasslands is believed to have been driven by a combination of factors including overgrazing, drought, variability in rainfall, and suppression of fire regimes Moreno-de las Heras et al. (2016). These shrubs are also thought to further facilitate their own encroachment through positive feedbacks (Grover and Musick, 1990; D’Odorico et al., 2012) by modifying their environment in ways that favor continued growth and recruitment, including changes to the local micro-climate (D’Odorico et al., 2010) and rates of soil erosion (Turnbull et al., 2010). Such positive feedback also involve suppression of herbaceous competitors, reducing competition as well as the amount of flammable biomass used to fuel the fires that keep creosotebush growth in check (Van Auken, 2000). We hypothesized that, given potential for positive feedback mechanisms, the rarity of conspecifics at the low-density encroachment front may depress demographic performance and generate pushed-wave dynamics.

104 We used a combination of observational and experimental data from shrub ecotones
 105 in central New Mexico to parameterize a spatial integral projection model (SIPM) that
 106 predicts that speed of encroachment (m/yr) resulting from lower-level demographic and
 107 dispersal processes. Our data came from demographic surveys and experimental trans-
 108 plants along replicate ecotone transects spanning a gradient of shrub density, and seed
 109 drop experiments to estimate the properties of the dispersal kernel. We focused on wind
 110 dispersal of seeds, since little is known about the natural history of dispersal in this
 111 system and the seeds lack rewards to attract animal dispersers. We also used re-surveys
 112 of permanents transects as an independent measure of encroachment that provided a
 113 benchmark against which to evaluate model predictions. The SIPM accounts for size-
 114 structured demography of creosotebush, allows us to test whether shrub expansion is
 115 pulled by the low-density front or pushed from the high-density core, and identifies the
 116 local (demographic) and spatial (seed dispersal) life cycle transitions that most strongly
 117 contribute to expansion speed². We address the following specific questions:

- 118 1. What is the nature of conspecific density dependence in demographic vital rates
 119 along shrub encroachment ecotones? Is encroachment pulled by the individuals at
 120 the front or pushed by individuals behind it?
- 121 2. What is the seed dispersal kernel for this species and how does this vary with
 122 maternal plant size?
- 123 3. What is the predicted rate of expansion from the SIPM and which lower-level
 124 processes most strongly affect the expansion speed?
- 125 4. How does the observed rate of encroachment in the recent past compare to model
 126 predictions?

²*we will need to stay consistent with the language of encroachment/expansion/invasion. For now I am swictihg a lot.*

127 **Materials and methods**

128 **Study species**

129 Creosotebush *Larrea tridentata* is a perennial, drought-resistant shrub that is native to
130 the arid and semiarid regions of the southwestern United States and northern Mexico.
131 High-density areas of creosotebush consist largely of barren soil between plants due to
132 the “islands of fertility” these shrubs create around themselves (Schlesinger et al., 1996;
133 Reynolds et al., 1999), though lower-density areas will often contain grasses in the inter-
134 shrub spaces (Fig. 1). In our northern Chihuahuan desert study region creosotebush
135 reproduces sexually, with numerous small yellow flowers giving rise to highly pubescent
136 spherical fruits several millimetres in diameter; these fruits consist of five carpels, each
137 of which contains a single seed. Seeds are dispersed from the parent plant by gravity and
138 wind, with the possibility for seeds to subsequently be transported by animals or water
139 (Maddox and Carlquist, 1985). In other regions, this species also reproduces asexually
140 and can give rise to long-lived clonal stands (Vasek, 1980), but this does not occur in our
141 study region. The foliage is dark green, resinous, and unpalatable to most grazing and
142 browsing animals (Mabry et al., 1978).

143 **Study site**

144 We conducted our work at the Sevilleta National Wildlife Refuge (SNWR), a Long-Term
145 Ecological Research (SEV-LTER) site in central New Mexico. The refuge exists at the in-
146 tersection of several eco-regions, including the northern Chihuahuan Desert, Great Plains
147 grassland, and steppes of the Colorado Plateau. Annual precipitation is approximately
148 250 mm, with the majority falling during the summer monsoon season from June to
149 September. The recruitment events that facilitate creosotebush expansion are thought
150 to be highly episodic (Peters and Yao, 2012), and this may be linked to fluctuations in
151 monsoon precipitation (Boyd and Brum, 1983; Bowers et al., 2004). Monsoon precipita-

tion during the study years (2013-2017) was [summarise climate data].

Demographic data

Ecotone transects

We collected demographic data during early June of every year from 2013-2017. This work was conducted at **four sites in the eastern part of SNWR**³ (one site was initiated in 2013 and the other three in 2014), with three transects at each site. All transects were situated along a shrubland-grassland ecotone so that a full range of shrub densities was captured: each transect spanned core shrub areas, grassland with no or few shrubs, and the transition between them. Lengths of these transects varied from 200 to 600 m, determined by the strength of vegetation transition since “steep” transitions required less length to capture the full range of shrub density.

We quantified shrub density in 5-meter “windows” along each transect, including all shrubs within one meter of the transect on either side (shrubs that partially overlapped with the census area were included). Densities were quantified once for each transect (in 2013 or 2014) and were assumed to remain constant for the duration of the study, a reasonable assumption for a species with very low recruitment and very high survival of established plants. Given the population’s size structure, we weighted the density of each window by the sizes of the plants, which we quantified as volume (cm³). Volume was calculated as that of an elliptic cone: $V_i = \frac{\pi h}{3} \frac{lw}{4}$ where l , w , and h are the maximum length, maximum width, and height, respectively. Maximum length and width were measured so that they were always perpendicular to each other, and height was measured from the base of the woody stem at the soil surface to the tallest part of the shrub. The weighted density for a window was then expressed as log(volume) summed over all plants in the window.

³*would a map be helpful?*

176 **Observational census**

177 At approximately 50-m intervals along each transect we tagged up to 10 plants for an-
178 nual demographic census and recorded their local (5-m resolution) window so that we
179 could connect individual demographic performance to local density. These tagged shrubs
180 were revisited every June and censused for survival (alive/dead), size (width, length, and
181 height, as above), flowering status, and fertility of flowering plants (numbers of flower-
182 buds, flowers, and fruits). In instances where shrubs had large numbers of reproductive
183 structures that would be difficult to reliably count (a large shrub may have thousands
184 of flowers or fruits), we made counts on a fraction of the shrub and extrapolated to es-
185 timate whole-plant reproduction. Creosotebush does not have one discrete reproductive
186 event per year; instead, flowering may occur throughout much of the warm season. By
187 combining counts of buds, flowers, and fruits we intended to capture a majority of the
188 season's reproductive output, assuming that all buds and flowers will eventually become
189 fruits. Our measurements of reproductive output are therefore conservative and may un-
190 derestimate total seed production for an entire transition year. Each year, we searched
191 for new recruits within one m on either side of the transect. New recruits were tagged
192 and added to the demographic census. The observational census included a total of 522
193 unique individuals.

194 **Transplant experiment**

195 We conducted a transplant experiment in 2015 to test how shrub density affects seedling
196 survival. This approach complemented observational estimates of density dependence
197 and filled in gaps for a part of the shrub life cycle that was rarely observed due to low
198 recruitment. Seeds for the experiment were collected from plants in our study popu-
199 lation in 2014. Seeds were germinated on Pro-Mix potting soil (Quakertown, PA) in
200 Fall 2014 and seedlings were transferred to 3.8 cm-by-12.7 cm cylindrical containers and
201 maintained in a greenhouse at Rice University. Seedlings were transported to SNWR

202 and transplanted into the experiment during July 27-31, 2015. Transplant timing was
203 intended to coincide with the monsoon season, when most natural recruitment occurs.

204 The transplant experiment was conducted at the same four sites and three transects
205 per site as the observational demographic census, where we knew weight shrub densities
206 at 5-m window resolution. We established 12 1-m by 1-m plots along each transect.
207 Plots were intentionally placed to capture density variation: four plots were in windows
208 with zero shrubs, four plots were placed in the top four highest-density windows on the
209 transect, and the remaining four plots were randomly distributed among the remaining
210 windows with weighted density greater than zero. Plots were placed in the middle of
211 each 5-m window (at meter 2.5) and were divided into four 0.5-m by 0.5-m subplots. We
212 divided each subplot into nine squares (0.125-m by 0.125-m) and recorded ground cover
213 of each square as one of the following categories: bare ground, creosotebush, black grama
214 (*B. eriopoda*), blue grama (*B. gracilis*), other grass, or “other”. Each subplot received one
215 transplanted shrub seedling, for a total of 48 transplants per transect, 144 transplants
216 per site, and 576 transplants in the entire experiment. Each site was set up on a different
217 day and there was a significant monsoon event after the third and before the fourth
218 site. This resulted in differential mortality that appears to be related to site (captured
219 as a statistical random effect) but more likely reflects the timing of the monsoon event
220 relative to planting (moist soil likely promoted transplant survival). We revisited the
221 transplant experiment on October 24, 2015 to survey mortality. After that first visit,
222 transplants were censused along with the naturally occurring plants each June, following
223 the methods described above.

224 **Demographic analysis**

225 We fit statistical models to the demographic data and used AIC-based model selection to
226 evaluate empirical support for alternative candidate models. The top statistical models
227 were then used as the vital rate sub-models of the SIPM, so there is a strong connection

228 between the statistical and population modeling, as is typical of integral projection mod-
229 eling. Our analyses focused on the following demographic vital rates: survival, growth,
230 probability of flowering, fertility (flower and fruit production), seedling recruitment, and
231 seedling size. Most of these vital rates were modeled as a function of plant size, and all
232 of them included the possibility of density dependence.

233 The alternative hypotheses of pushed versus pulled wave expansion rest on how the
234 rate of population increase (λ), derived from the combination of all vital rates, respond
235 to density. We were particularly interested in whether demographic performance was
236 maximized as local density goes to zero (pulled) or at non-zero densities behind the
237 wave front (pushed). To flexibly model density dependence and detect non-monotonic
238 responses, we used generalized additive models in the R package ‘mgcv’ (Wood, 2017).
239 For each vital rate, we fit candidate models with or without a smooth term for local
240 weighted density (among other possible covariates). To avoid over-fitting, we set the
241 ‘gamma’ argument of `gam()` to 1.8, which increases the complexity penalty, results in
242 smoother fits (Wood, 2017), and makes our approach more conservative (other gamma
243 values yielded qualitatively similar results). We pooled data across transition years for
244 analysis. All models included the random effect of transect (12 transects across 4 sites);
245 we did not attempt to model both site and transect-within-site random effects due to the
246 low numbers of each. All vital rate functions used the natural logarithm of volume (cm^3)
247 as the size variable and the sum of $\log(\text{volume})$ as the weighted density of a transect
248 window.

249 **Survival** We modeled survival or mortality in year $t+1$ as a Bernoulli random variable
250 with three candidate models for survival probability. These included smooth terms for
251 initial size in year t only (1), initial size and weighted density (2), and both smooth terms
252 plus an interaction between initial size and weighted density (3). We analyzed survival of
253 experimental transplants and observational census plants together in the same analyses,

with a fixed effect of transplant status (yes/no) included in all candidate models. Since recruits and thus mortality events were both very rare in the observational survey, this approach allowed us to “borrow strength” over both data sets to generate a predictive function for size- and possibly density-dependent survival while statistically accounting for differences between experimental and naturally occurring plants. Because we had additional, finer-grained cover data for the transplant experiment that we did not have for the observational census, we conducted an additional stand-alone analysis of transplant survival that explored the influence of covariates at multiple spatial scales (Appendix).

Growth We modeled size in year $t + 1$ as a Gaussian random variable. There were nine candidate models for growth. The simplest model (1) defined the mean of size in year $t + 1$ as a smooth function of size in year t and constant variance. Models (2) and (3) had constant variance but the mean included smooth terms for initial size and weighted density (2) or both smooth terms plus an interaction between initial size and weighted density (3). Models 4-6 had the same mean structure as 1-3 but defined the standard deviation of size in year $t + 1$ as a smooth function of initial size. Models 7-9 mirrored 4-6 and additionally included a smooth term for weighted density in the standard deviation. Modeling growth correctly is important because it defines the probability of any future size conditional on current size, a critical element of the IPM transition kernel. We verified that the AIC-selected model described the data well by simulating data from it and comparing the moments (mean, variance, skewness, and kurtosis) of simulated and real data.

Flowering and fruit production We modeled shrub reproductive status (vegetative or flowering) in year t as a Bernoulli random variable with three candidate models for flowering probability. These included smooth terms for current size (in year t) only (1), size and weighted density (3), and both smooth terms plus an interaction between size and weighted density. We modeled the reproductive output of flowering plants (the sum

of flowerbuds, open flowers, and fruits) in year t as a negative binomial random variable. There were three candidate models for mean reproductive output that corresponded to the same three candidates for flowering probability.

Recruitment and recruit size We modeled seedling recruitment in each transect window as a binomial random variable given the number of total seeds produced in that window in the preceding year. There were two candidate models, with and without an influence of weighted density on the per-seed recruitment probability. To estimate window-level seed production, we used the best-fit models for flowering and fruit production and applied this to all plants in each window that we observed in our initial density surveys. We assume that recruits come from the previous year's seeds and not from a long-lived soil seed bank.

We modeled recruit size as a Gaussian-distributed random variable and fit four candidate models including an influence of weighted density on mean, variance, both, and neither.

Density-dependent IPM

The size- and density-dependent statistical models comprised the sub-models of a density dependent Integral Projection Model (IPM) that we used to evaluate how the shrub population growth rate responded to con-specific density; we present this non-spatial model before layering on the spatial dynamics generated by seed dispersal. A basic density-independent IPM predicts the number of individuals of size x' at time $t + 1$ ($n(x', t + 1)$) based on a projection kernel (K) that gives the rates of transition from sizes x to x' from times t to $t + 1$ and is integrated over the size distribution from the minimum (L) to maximum (U) sizes. In a density-dependent IPM, components of the

303 projection kernel may respond to population abundance and structure:

$$304 \quad n(x', t + 1) = \int_L^U K(x', x, \tilde{n}(t)) n(x, t) dx \quad (1)$$

305 Here, $\tilde{n}(t)$ is some function of population structure $n(x, t)$ such as the total density
 306 of conspecifics ($\tilde{n}(t) = \int n(x, t) dx$) or, as in our case, total density weighted by size
 307 ($\tilde{n}(t) = \int x n(x, t) dx$). For simplicity, in the analyses that follow we do not model density
 308 as a dynamic state variable; instead, we treat density as a static covariate ($\tilde{n}(t) = \tilde{n}$) and
 309 evaluate the IPM at a range of density values. As in our statistical modeling, the size
 310 variable of the IPM (x, x') was $\log(\text{cm}^3)$.

311 For our model, the size- and density-dependent demographic transitions captured by
 312 the projection kernel include growth or shrinkage (g) from size x to x' conditioned on
 313 survival (s) at size x (combined growth-survival function $G(x', x, \tilde{n}) = g(x', x, \tilde{n})s(x, \tilde{n})$),
 314 and the production of new size- x' individuals from size- x parents ($Q(x', x, \tilde{n})$). Repro-
 315 duction reflects the probability of flowering at size x (p), the number of seeds produced
 316 by flowering plants (d), the per-seed probability of recruitment (r), and the size distri-
 317 bution of recruits (c). Collectively, the rate at which x -sized individuals produce x' -sized
 318 individuals at density \tilde{n} is given by the combined reproduction-recruitment function
 319 $Q(x', x, \tilde{n}) = p(x, \tilde{n})d(x, \tilde{n})r(\tilde{n})c(x', \tilde{n})$. Thus, we can express the projection kernel as:

$$320 \quad K(x', x, \tilde{n}) = G(x', x, \tilde{n}) + Q(x', x, \tilde{n}) \quad (2)$$

321 For analysis, we evaluated the IPM kernel over a range of local densities from the min-
 322 imum to the maximum of weighted density values from the 5-meter windows ($0 \leq \tilde{n} \leq$
 323 \tilde{n}_{max}). At each density level, we discretized the IPM kernel into a 200×200 approximat-
 324 ing matrix and calculated the asymptotic growth rate $\lambda(\tilde{n})$ as its leading eigenvalue. We
 325 extended the lower (L) and upper (U) integration limits to avoid unintentional “eviction”
 326 using the floor-and-ceiling method (Williams et al., 2012).

327 We sought to characterize the shape of density dependence: whether fitness declined
 328 monotonically or not with increasing density. We quantified uncertainty in the density-
 329 dependent growth rate $\lambda(\tilde{n})$ by bootstrapping our data. For each bootstrap, we randomly
 330 sampled 75% of our demographic data, re-ran the statistical modeling and model selec-
 331 tion, and used the top vital rate models to generate $\lambda(\tilde{n})$ for that data subset. We
 332 repeated this procedure for 500 bootstrap replicates.

333 Dispersal modelling

334 **WALD dispersal model** Dispersal kernels were calculated using the WALD, or Wald
 335 analytical long-distance dispersal, model that uses a mechanistic approach to predict
 336 dispersal patterns of plant propagules by wind. The WALD model, which is based in fluid
 337 dynamics, can serve as a good approximation of empirically-determined dispersal kernels
 338 (Katul et al., 2005; Skarpaas and Shea, 2007) and may be used when direct observations
 339 of dispersal are not available. Under the assumptions that wind turbulence is low, wind
 340 flow is vertically homogenous, and terminal velocity is achieved immediately upon seed
 341 release, the WALD model simplifies a Lagrangian stochastic model to create a dispersal
 342 kernel that estimates the likelihood a propagule will travel a given distance (Katul et al.,
 343 2005). Our dispersal kernel takes the form of the inverse Gaussian distribution

$$344 \quad p(r) = \left(\frac{\lambda'}{2\pi r^3} \right)^{\frac{1}{2}} \exp \left[-\frac{\lambda'(r - \mu')^2}{2\mu'^2 r} \right] \quad (3)$$

345 that is a **slight adaptation**⁴ from equation 5b in Katul et al. (2005), using r to denote
 346 dispersal distance. Here, λ' is the location parameter and μ' is the scale parameter, which
 347 depend on environmental and plant-specific properties of the study system. (We use λ'
 348 for consistency with notation in related papers, but λ' the dispersal location parameter
 349 should not be confused with λ the geometric growth rate.) The location and scale
 350 parameters are defined as $\lambda' = (H/\sigma)^2$ and $\mu' = HU/F$; these are functions of the height

⁴*unclear what this refers to*

351 H of seed release, wind speed U at seed release height, seed terminal velocity F , and
 352 the turbulent flow parameter σ that depends on both wind speed and local vegetation
 353 roughness. We parameterized the WALD dispersal kernel using windspeed data from
 354 the SEV-LTER weather station nearest our study site (Moore and Hall, 2022) and seed
 355 terminal velocity data from laboratory-based seed-drop experiments. Methods for our
 356 seed data collection and technical details of dispersal kernel modeling are provided in
 357 Appendix A.

358 **Spatial integral projection model**

359 We used a spatial integral projection model to piece together seed dispersal and density-
 360 dependent demography, and generate predictions for the rate of shrub expansion that
 361 results from this combination of local and spatial processes. The spatially explicit model
 362 builds upon the non-spatial model (Eq. 1) and adds a spatial variable (z, z') such
 363 that demographic transitions occur across both time and space according to a combined
 364 demography-dispersal kernel \tilde{K} :

$$365 \quad n(x', z', t + 1) = \int_{-\infty}^{+\infty} \int_L^U \tilde{K}(x', x, z', z, \tilde{n}(z, t)) n(x, z, t) dx dz \quad (4)$$

366 Here, $\tilde{K}(x', x, z', z, \tilde{n}(z, t))$ is the rate of transition from size x and location z to size x'
 367 and location z' given density $\tilde{n}(z, t)$ at location z . As before, \tilde{n} is a function of pop-
 368 ulation structure – in our model, weighted local density – but here integrated over an
 369 explicit competitive “neighborhood”: $\tilde{n}(z, t) = \int_{z-h}^{z+h} \int_L^U x n(x, z, t) dx dz$ where h repre-
 370 sents neighborhood size in the units of z .

371 Given that the shrub population at this site is approximately homogeneous perpen-
 372 dicular to the direction of encroachment, expansion is modelled as a wave moving in one
 373 dimension. A spatial integral projection model (SIPM) is used to estimate the speed at
 374 which encroachment occurs; such a model incorporates the effects of variation in traits

like plant size that stage-structured models, such as those described in Neubert and Caswell (2000), do not capture. According to Jongejans et al. (2011), a general SIPM can be formulated as

$$\mathbf{n}(x_2, z_2, t + 1) = \iint \tilde{K}(x_2, x_1, z_2, z_1) \mathbf{n}(x_1, z_1, t) dx_1 dz_1 \quad (5)$$

where x_1 and x_2 are locations of individuals of a particular size before and after one unit of time, and z_1 and z_2 are the respective sizes. The vector \mathbf{n} indicates the population density of each size, and \tilde{K} is a kernel that combines dispersal with demography. Though this SIPM represents a continuous spectrum of shrub sizes and densities, it was implemented by discretising the above integral with a 200 x 200 matrix, as this makes calculations significantly more tractable.

Movement of the wave is determined by the components of the combined dispersal/demography kernel \tilde{K} , which is of the same form as that used in Jongejans et al. (2011). Here,

$$\tilde{K}(x_2, x_1, z_2, z_1) = K(x_2 - x_1)Q(z_2 - z_1) + \delta(x_2 - x_1)G(z_2 - z_1) \quad (6)$$

and K is the dispersal kernel, Q a reproduction function, G a growth function, and δ the Dirac delta function. G is derived from the model for annual growth ratio, and Q is derived from the reproductive structures model as well as other factors including number of seeds per reproductive structure, probability of recruitment from seed, and recruit size. Both G and Q give the probability of transition between sizes; in the case of G , this is the probability of growing from one specific size to another, and in the case of Q the probability that an individual of a specific size produces a recruit of a specific size. The product of K and Q represents the production and dispersal of motile propagules, while the product of G and δ represents the growth of sessile individuals.

Assuming strictly negative density dependence (i.e., pulled waves), the speed of the

moving wave can be calculated as

$$c^* = \min_{s>0} \left[\frac{1}{s} \ln(\rho_s) \right] \quad (7)$$

where s is the wave shape parameter and ρ_s is the dominant eigenvalue of the kernel \mathbf{H}_s (Jongejans et al., 2011). The kernel \mathbf{H}_s is defined as

$$\mathbf{H}_s = M(s)Q(z_2 - z_1) + G(z_2 - z_1) \quad (8)$$

where $M(s)$ is the moment-generating function of the dispersal kernel (Jongejans et al., 2011). For one-dimensional dispersal, this moment-generating function can be estimated as

$$M(s) = \frac{1}{N} \sum_{i=1}^n I_0(sr_i) \quad (9)$$

where r is the dispersal distance for each observation, and I_0 is the modified Bessel function of the first kind and zeroth order (Skarpaas and Shea, 2007). In order to obtain M , numerous dispersal distances were simulated from the dispersal kernel $K(r)$ described in the previous section, with over 2000 replications for each shrub height increment of 1 cm. This was performed over the range from the lowest possible dispersal height to the maximum shrub height. Once $M(s)$ was obtained for dispersal at each shrub height, \mathbf{H}_s and c^* were calculated for each value of s ; this was done for values of s ranging from 0 to 2, as it is this range in which c^* occurs.

Estimates of the wavespeed were bootstrapped for a total of 1000 replicates. Each bootstrap replicate recreated size- and density-dependent demographic models using 80% resampling on the original demographic data, and recreated dispersal kernels also using 80% resampling on the wind speeds and seed terminal velocities. Between replicates, the structure of the demographic models was kept constant, though coefficient estimates were not; this approach, while effectively ignoring model uncertainty, has the benefit of

422 increasing computational efficiency, which is especially useful given the time-consuming
423 nature of numerically estimating the many dispersal kernels used in the model.

424 **Encroachment re-surveys**

425 We recorded shrub percent cover along two permanent 1000-m transects that spanned
426 the shrub-grass ecotone, from high to low to near-zero shrub density. These surveys were
427 conducted in summer 2001 and again in summer 2013 to document change in creosotebush
428 abundance and spatial extent. At every 10 meters, shrub cover was recorded in nine cover
429 classes ($<1\%$, $1-4\%$, $5-10\%$, $10-25\%$, $25-33\%$, $33-50\%$, $50-75\%$, $75-95\%$, $>95\%$). For
430 visualization, we show midpoint values of these cover classes at each meter location for
431 both transects and years.

432 **Results**

433 **Size and density dependent demography**

434 Demographic data from naturally occurring and transplanted individuals revealed strong
435 size- and density-dependence in demographic vital rates. For most sizes and vital rates,
436 local density had negative demographic effects. Statistical support for size- and density-
437 dependence is provided in Table XX, which provides AIC rankings for candidate models
438 based on the completed (not bootstrapped) data set.

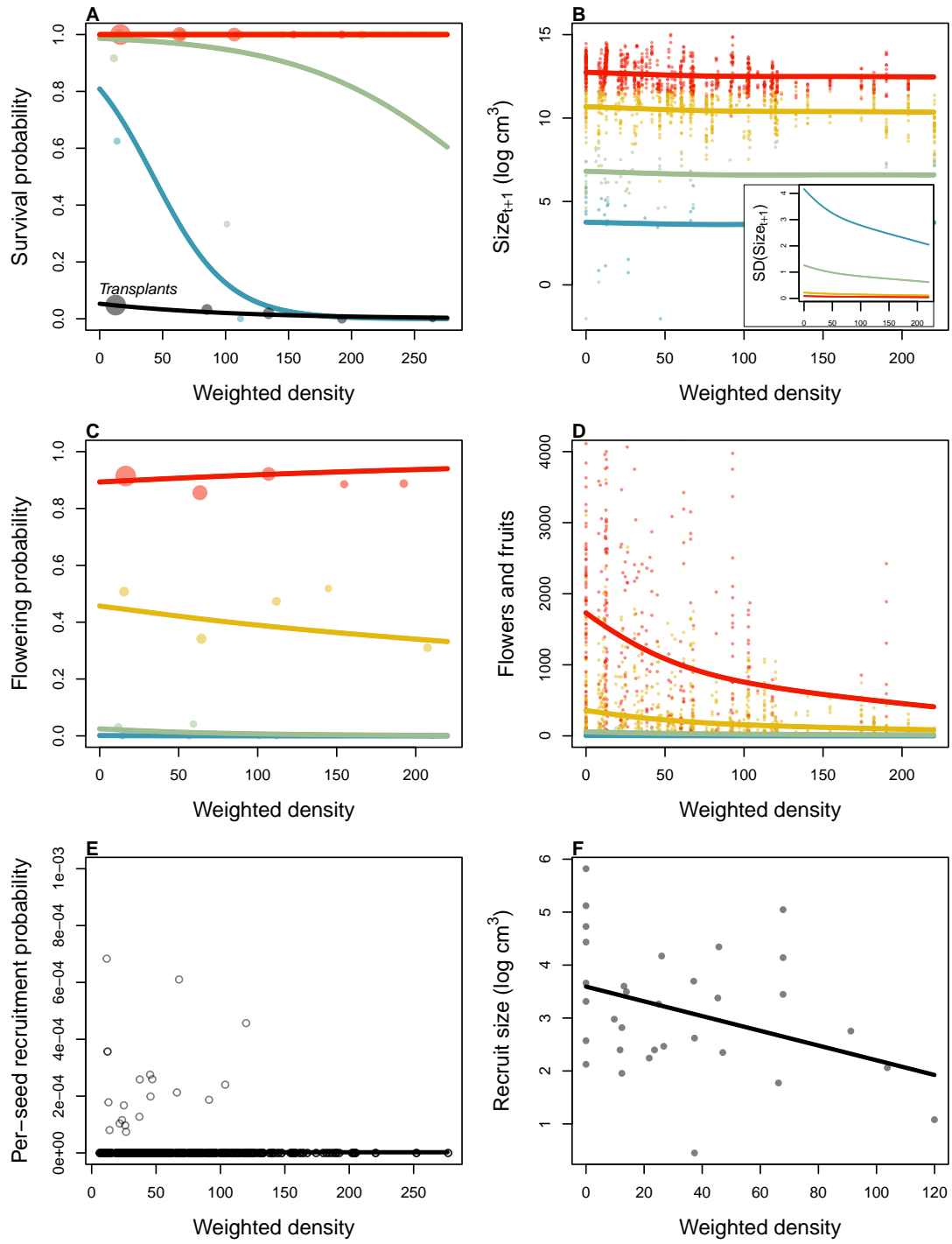


Figure 2: Size- and density-dependence in demographic vital rates. **A** Probability of survival from natural population census and transplant experiment (black line), **B** Mean and variance (inset) of size conditional on previous size, **C** Probability of flowering, **D** Flower and fruit production, **E** Probability of recruitment per seed, **F** Recruit size. In **A–E**, colored lines indicate four size groups (red is largest, blue is smallest), discretized for data visualization only. In all panel, weighted density is the sum of all plant sizes $\log(\text{cm}^3)$ within the same 5-m window as the census individual.

Survival Among naturally occurring plants, survival of large, established individuals was very high (Fig. 2A). We observed relatively few mortality events (XX out of XX) and nearly all of these were among new recruits. The probability of survival at these small sizes declined with increasing density.

Survival of transplants was very low, lower even than survival of similarly-sized, naturally occurring recruits (Fig. 2B). However, the transplant results support the general pattern of negative density dependence in survival. Among the XX survivors, XX of them occurred in transect windows in the bottom 10th percentile of weighted shrub density.

SHORT PARAGRAPH SUMMARIZING SMALLER-SCALE ANALYSIS IN APPENDIX.

Growth Current size was strongly predictive of future size, as expected, and there was weak negative density dependence in mean future size conditioned on current size (Fig. 2C). However, there was a stronger signal of density dependence in the variance of future size (Fig. 2C, inset). Plants at low density exhibited greater variance in growth trajectories and this was especially true at the smallest sizes. Thus, large increases in the size of new recruits were most likely to occur under low-density conditions.

Flowering and fruit production Flowering probability was strongly size-dependent and very weakly sensitive to local density (Fig. 2D). However, fertility of flowering plants was strongly negative density dependent, with greatest flower and fruit production by the largest plants at the lowest densities, and vice versa (Fig. 2E).

Recruitment and recruit size We observed XX natural recruitment events along our transects during the study years and our estimate recruitment rate, given total expected seed production in each window preceding the recruitment year, was very low ($\leq XX$, 2F). While most recruitment events occurred at low density, this is also where most seed production was concentrated (Fig. 2E) and low-density windows were over-represented

relative to high density. For these reasons we were more likely to observe recruitment events at low density. Controlling for sampling effort and seed production, the statistical models indicated that our data were most consistent with a constant, density-independent recruitment rate (Table XX). However, the mean size of new recruits declined significantly with local density (Fig. 2F).

Population growth rate As expected based on the vital rate results, the asymptotic population growth rate λ declined monotonically with density (Fig. 3). This was true across all bootstrap replicates, indicating high certainty that shrub fitness is maximized at zero density and thus that the expansion wave is “pulled”. Mean growth rate at low density was XX% per year, with bootstrap uncertainty spanning 1–6%. At high density population growth rates approached $\lambda = 1$, indicating stasis driven by near-perfect survival and extremely rare recruitment.

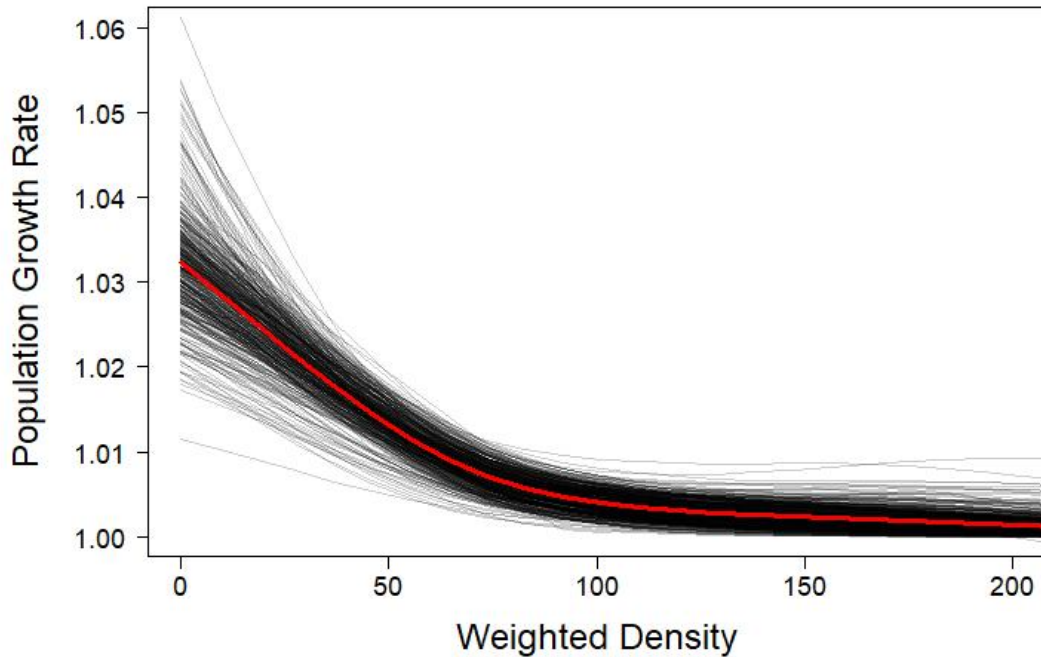


Figure 3: Density dependence in the asymptotic geometric growth rate (λ). Lines show bootstrap replicates sub-sampled from the full demographic data set. Weighted deighted density is the sum of all plant sizes $\log(cm^3)$ within 5-m windows.

476 The speed of encroachment at the study site as estimated by the SIPM is rather
 477 slow; as can be seen in Figure 4, the low-density wavefront moves at approximately
 478 0.5 cm/yr under normal conditions and at 1 cm/yr under the best seedling survival
 479 conditions observed in the dataset. These improved conditions were observed due to
 480 above-average rainfall that occurred after greenhouse-grown seedlings were transplanted
 481 to the site. Population growth in this low-density region of the moving wave is also low,
 482 with a geometric growth rate of $\lambda \approx 1.006$ and even lower rates of growth the higher-
 483 density regions behind; in the higher-survival scenario the maximum rate increases to
 484 $\lambda \approx 1.013$, with growth still decreasing as density increases. For both scenarios, the
 485 decrease in population growth rate with increasing density was monotonic across the

range of observed standardised densities, as is shown in Figure 4. This suggests that an Allee effect is likely not present in this population, as the highest rate of population growth is found at the lowest density vanguard of the encroaching population. Thus, the conditions necessary for equation 9 to be valid are satisfied, and these wavespeeds are applicable for a pulled-wave scenario in which no Allee effects are present.

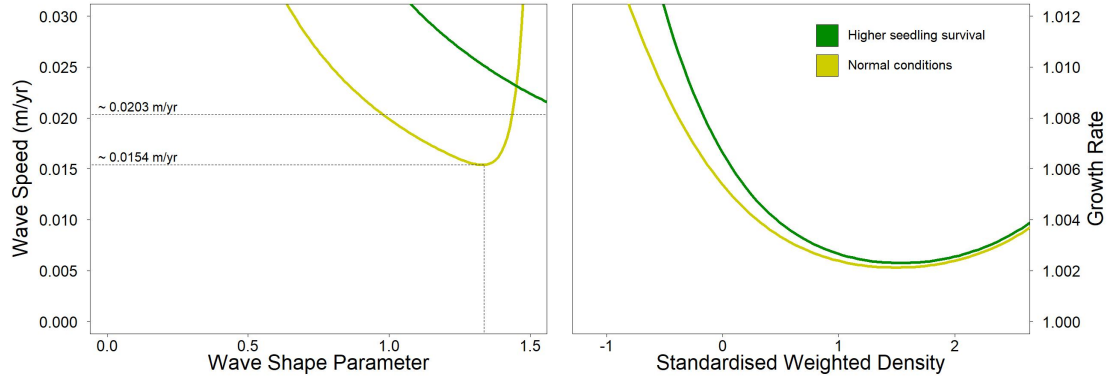


Figure 4: Estimated encroachment wave speeds (left) and geometric rates of population growth (right) for higher post-rainfall seedling survival and normal conditions.

As the speed of encroachment is quite limited, so is the extent of wind dispersal. Long distance dispersal events, while more common for taller shrubs than their shorter counterparts, are still uncommon overall. For the tallest shrub height of 1.98 m, only 0.32% of propagules exceed a dispersal distance of 5 m, and 0.02% exceed 10 m. At 1 m, or approximately half the tallest shrub height, long distance dispersal is even less likely, with 0.0046% of propagules exceeding a dispersal distance of 5 m and 0.0009% exceeding 10 m. Given that the median shrub height is only 0.64 m, the occurrence of long-distance wind dispersal in most of the shrub population is highly improbable, and the few instances in which it occurs will only be limited to the tallest shrubs. Thus, as Figure 5 demonstrates, shorter dispersal distances dominate; even for the tallest shrub, 81% of seeds fall within only a metre of the plant, and this percentage increases as shrub height decreases. Dispersal kernels have their highest probability density at dis-

503 persal distances between 2 and 8 cm from the shrub; here, as shrub height increases, the
 504 most probable dispersal distance slightly increases while maximum probability density
 505 decreases. Regardless of the shrub height, most dispersal will occur very close to the
 506 plant, though increases in shrub height dramatically increase the likelihood of dispersal
 507 at longer distances. It is clear that the shape of the height-dependent dispersal kernel
 508 $K(r)$ varies greatly among the shrub population given the large range of shrub heights
 509 observed; shrubs at lower heights have more slender kernels with most of the seeds dis-
 510 persing closer to the plant, while taller shrubs have kernels with much fatter tails and
 511 are more capable of longer-distance dispersal.

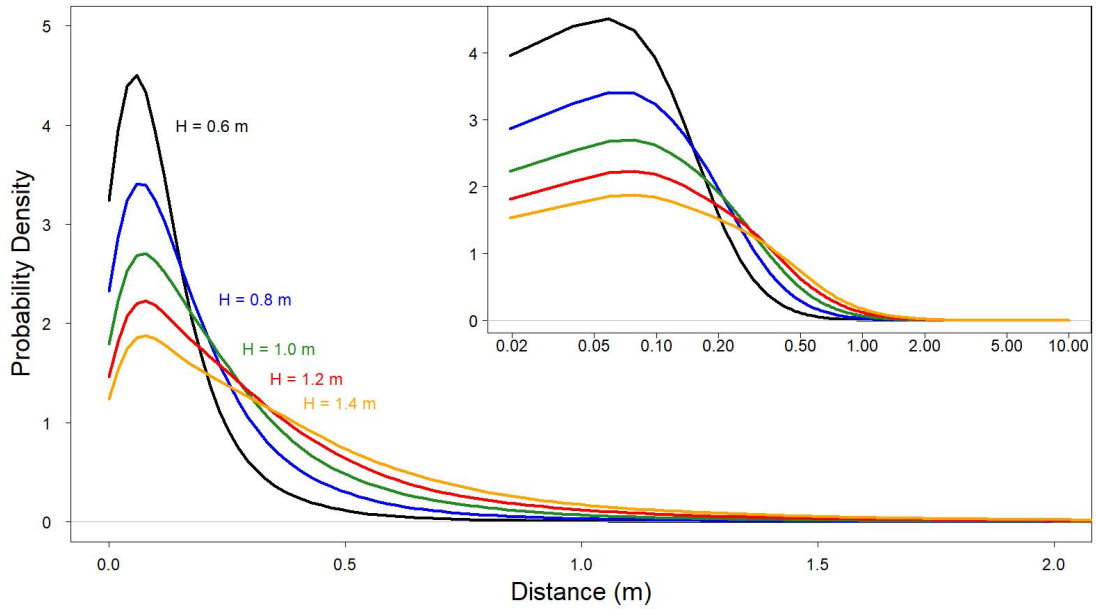


Figure 5: Dispersal kernels, with each colour representing a selected shrub height. The inset plot is the same as the large plot, though with a logarithmic x-axis to more easily show differences in dispersal probability at smaller distances.

512 Density and size dependence are evident in all 4 of the demographic rates, with
 513 coefficients for each model displayed in Table 2. For growth, reproduction, and survival,
 514 density dependence is mostly negative and monotonic; this is not the case for probability

515 of flowering, where shrub size seems to be more important than the effects of density alone
516 and suggests that larger shrubs have a higher probability of flowering than their smaller
517 counterparts. This, along with size and density dependence in growth and reproduction,
518 is shown in Figure 6. Size dependence is positive for reproduction, as would be expected
519 since larger plants typically produce more flowers and fruits. However, annual growth
520 decreases as size increases; this could be in part due to the annual growth in this study
521 being quantified as a proportion relative to the shrub's initial size. While larger shrubs
522 may produce more plant material over a year in terms of absolute volume, smaller shrubs
523 produce less but can still have higher annual growth in terms of the percentage of volume
524 added relative to their initial volume. When compared to density, shrub size is a much
525 stronger predictor of survival, with significant differences in mortality rates depending on
526 shrub size. For small shrubs, mortality is exceptionally high, and increases in volume for
527 these shrubs only slightly increase the likelihood of survival. However, after shrubs reach
528 a logarithmic volume of approximately 7.3, they are almost guaranteed to survive, with
529 survival rates near 100% persisting regardless of any further size increases. Interestingly,
530 though most recruits were found at lower densities, the probability of recruitment from
531 seed displays positive density dependence; the probability of recruitment was still very
532 low, though, with a baseline rate of approximately 2 recruits per 10,000 seeds.

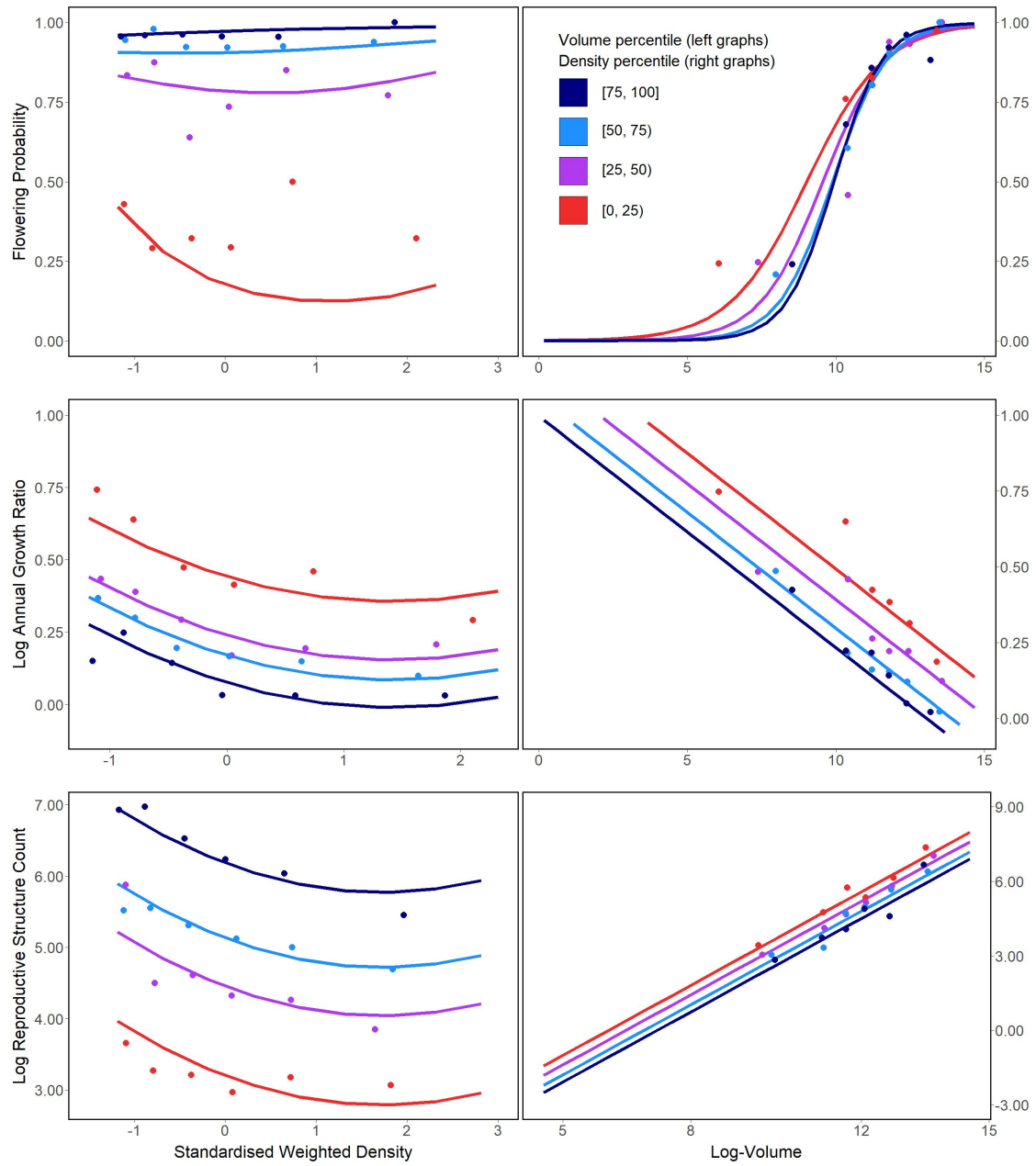


Figure 6: Flowering probability (top row), log annual growth ratio (centre row), and log reproductive structure count (bottom row) at all four sampling sites. In the left column of graphs, the three response variables are shown as a function of density for each of four volume quartiles, with each quartile containing six density bins; in the right column, the opposite occurs, with response variables shown as functions of four volume quartiles that each contain six density bins. Graphs quantifying the number of reproductive structures include data only on plants that flowered.

533 Encroachment re-surveys

534 Re-surveys along two permanent transects revealed virtually no change the in the creosote
535 expansion wave over 12 years (Fig. 7). There were local changes in percent cover: on
536 average cover increased by XX% between surveys. However, there was no clear indication
537 that the leading edge of the creosote shrubland has advanced (the modest right-ward shift
538 on both transects is within the range of measurement error).

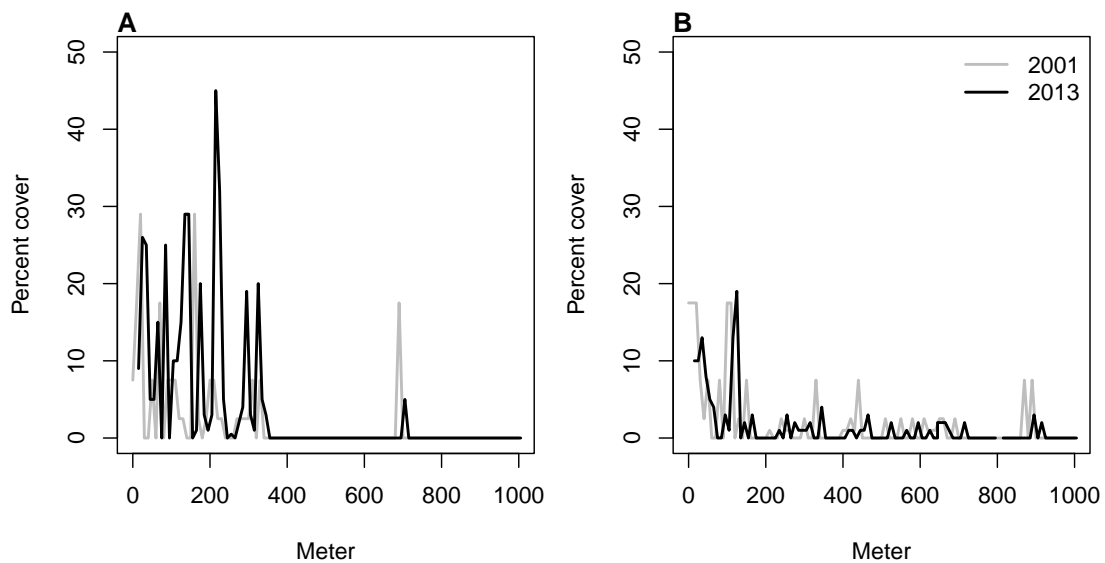


Figure 7: Re-surveys of shrub cover along two permanent trasects (A,B) surveyed in 2001 and 2013.

539 Discussion

540 The slow movement of the encroaching creosotebush wave at the Sevilleta LTER site
541 can likely be contributed to a combination of three factors: short dispersal distances
542 with extremely limited long-distance dispersal events, very low probability of recruit-
543 ment from seed, and high seedling mortality. These three barriers, when combined, form
544 a formidable challenge to the establishment of new shrubs at the low-density front of
545 the wave. First, a seed must travel far enough to avoid competition with the parent

shrub, which is unlikely given the dispersal kernels shown in Figure 2. Even if the seed manages to be dispersed this far, its chances of becoming a seedling are low. Caching and consumption by seed-eaters such as a variety of seed-harvesting ants (Whitford, 1978; Whitford et al., 1980; Lei, 1999) and the kangaroo rat *Dipodomys merriami* (Chew and Chew, 1970) decreases the amount of seeds available for germination. However, reduction in germination caused by destruction of seeds may be partly mitigated by the more favourable germination conditions that these seeds can experience when cached underground (Chew and Chew, 1970). Many of the remaining seeds will still fail to germinate, and in the unlikely event that germination does occur, seedlings will likely die given the high rates of mortality observed in smaller shrubs. Such high rates of creosotebush seedling mortality have been observed in other studies as well (Boyd and Brum, 1983; Bowers et al., 2004), probably due to a combination of herbivory, competition, and abiotic stresses.

However, as low as they are, the wavespeed estimates given in this paper are still conservative estimates for reasons mostly related to dispersal. First, it is important to note that the dispersal kernels used here, while they account for variation in factors such as wind speed and terminal velocity, may underestimate the distances that shrub propagules travel. Because the WALD model assumes that terminal velocity is reached immediately upon seed release, seeds in the estimate thus take a shorter time to fall and have less time to be transported by wind, and the true frequency of long-distance dispersal events may thus be greater than what is estimated here. Second, dispersal at the study site could occur through additional mechanisms other than wind. For example, secondary dispersal through runoff from significant rainfall events can transport seeds (Thompson et al., 2014), and given that long-distance dispersal by bird and subsequent species divergence is thought to be responsible for creosotebush being in North America in the first place (Wells and Hunziker, 1976), short-distance dispersal by other animals at the study site likely occurs. As mentioned above, seeds are transported by seed-

573 harvesting ants and granivorous mammals, where they are often stored in caches that
574 can be appreciable distances from the parent shrubs. Whether transportation occurs via
575 ant or rodent, creosotebush seeds can be moved significantly further than wind alone
576 can, though many of these seeds are eventually consumed.

577 Despite the more conservative estimates our model yields, the estimated rate of dis-
578 persal in creosotebush populations at the Sevilleta National Wildlife Refuge is consistent
579 with observations from the past 50-60 years, as creosotebush expansion during this time
580 has been minimal (Moreno-de las Heras et al., 2016). However, it cannot explain the
581 long-term increases in creosotebush cover at the study site, as total encroachment over
582 the past 150 years is much greater than what would be expected given the encroachment
583 rates derived by our models. Such a discrepancy is likely due to much of the expansion
584 occurring in an episodic fashion, with short times during which rapid encroachment oc-
585 curs due to favourable environmental conditions. This could be due in part to seedling
586 recruitment, which is a factor that strongly limits creosotebush expansion, being rare
587 and episodic. For example, Allen et al. (2008) estimate that a major recruitment event
588 occurred at this site in the 1950s, which is supported by photographic evidence from
589 Milne et al. (2003) of a drought-driven expansion during this time. Moreno-de las Heras
590 et al. (2016) estimate that after this expansion, several smaller creosotebush recruitment
591 events occurred in decadal episodes. However, such events can be highly localised and
592 may not necessarily occur at the low-density front of encroachment, which could explain
593 how these recruitment events can still coexist with lack of encroachment in the recent
594 past.

595 Overall, our observations and model highlight three aspects of creosotebush encroach-
596 ment that should be the focus of future studies seeking to obtain better estimates of
597 encroachment rates. First, negative density dependence in survival, growth, and repro-
598 duction is demonstrated, along with size dependence. The clear dependence on size and
599 conspecific density suggests that they both should be considered when estimating cre-

600 osotebush expansion and quantifying the demographic variation that contributes to it.
601 Second, wind dispersal in these shrubs is quite limited; though the dispersal kernels seen
602 here are typical in the sense that they are characterised by high near-plant dispersal and
603 exceptionally low long-distance dispersal, the scale across which such dispersal occurs
604 is small, with most seeds landing within only 1 m of the shrub. Wind dispersal alone
605 may be an underestimate of the true amount of dispersal occurring, and future work
606 should seek to incorporate the effects of dispersal by runoff and animals so that a more
607 representative model of total dispersal can be obtained. Finally, encroachment is slow or
608 even stagnates, but only most of the time. Though our encroachment speed estimates
609 are representative of creosotebush populations for most years, the significant expansion
610 seen over larger time scales suggests that there is episodic expansion in other years; while
611 our model is consistent with the recent stagnation in creosotebush encroachment at the
612 Sevilleta LTER site, a model that also includes interannual variability in factors such
613 as survival and recruitment would be able to better account for instances of episodic
614 population expansion that are characteristic of this location.

615 **Acknowledgements**

616 **Author contributions**

617 **Data accessibility**

618 **References**

- 619 Allen, A., W. Pockman, C. Restrepo, and B. Milne. 2008. Allometry, growth and
620 population regulation of the desert shrub *Larrea tridentata*. *Functional Ecology* pages
621 197–204.
- 622 Bowers, J. E., R. M. Turner, and T. L. Burgess. 2004. Temporal and spatial patterns in

623 emergence and early survival of perennial plants in the Sonoran Desert. *Plant Ecology*
624 **172**:107–119.

625 Boyd, R. S., and G. D. Brum. 1983. Postdispersal reproductive biology of a Mojave Desert
626 population of *Larrea tridentata* (Zygophyllaceae). *American Midland Naturalist* pages
627 25–36.

628 Brandt, J. S., M. A. Haynes, T. Kuemmerle, D. M. Waller, and V. C. Radeloff. 2013.
629 Regime shift on the roof of the world: Alpine meadows converting to shrublands in
630 the southern Himalayas. *Biological Conservation* **158**:116–127.

631 Buffington, L. C., and C. H. Herbel. 1965. Vegetational changes on a semidesert grassland
632 range from 1858 to 1963. *Ecological monographs* **35**:139–164.

633 Bullock, J. M., S. M. White, C. Prudhomme, C. Tansey, R. Perea, and D. A. Hooftman.
634 2012. Modelling spread of British wind-dispersed plants under future wind speeds in
635 a changing climate. *Journal of Ecology* **100**:104–115.

636 Cabral, A., J. De Miguel, A. Rescia, M. Schmitz, and F. Pineda. 2003. Shrub encroach-
637 ment in Argentinean savannas. *Journal of Vegetation Science* **14**:145–152.

638 Chew, R. M., and A. E. Chew. 1970. Energy relationships of the mammals of a desert
639 shrub (*Larrea tridentata*) community. *Ecological Monographs* pages 2–21.

640 D’Odorico, P., J. D. Fuentes, W. T. Pockman, S. L. Collins, Y. He, J. S. Medeiros,
641 S. DeWekker, and M. E. Litvak. 2010. Positive feedback between microclimate and
642 shrub encroachment in the northern Chihuahuan desert. *Ecosphere* **1**:1–11.

643 D’Odorico, P., G. S. Okin, and B. T. Bestelmeyer. 2012. A synthetic review of feedbacks
644 and drivers of shrub encroachment in arid grasslands. *Ecohydrology* **5**:520–530.

645 Gandhi, S. R., E. A. Yurtsev, K. S. Korolev, and J. Gore. 2016. Range expansions
646 transition from pulled to pushed waves as growth becomes more cooperative in an

647 experimental microbial population. *Proceedings of the National Academy of Sciences*
648 **113**:6922–6927.

649 Gardner, J. L. 1951. Vegetation of the creosotebush area of the Rio Grande Valley in
650 New Mexico. *Ecological Monographs* **21**:379–403.

651 Gibbens, R., R. McNeely, K. Havstad, R. Beck, and B. Nolen. 2005. Vegetation changes
652 in the Jornada Basin from 1858 to 1998. *Journal of Arid Environments* **61**:651–668.

653 Goslee, S., K. Havstad, D. Peters, A. Rango, and W. Schlesinger. 2003. High-resolution
654 images reveal rate and pattern of shrub encroachment over six decades in New Mexico,
655 USA. *Journal of Arid Environments* **54**:755–767.

656 Grover, H. D., and H. B. Musick. 1990. Shrubland encroachment in southern New Mexico,
657 USA: an analysis of desertification processes in the American Southwest. *Climatic*
658 *change* **17**:305–330.

659 Hsieh, C.-I., and G. G. Katul. 1997. Dissipation methods, Taylor’s hypothesis, and
660 stability correction functions in the atmospheric surface layer. *Journal of Geophysical*
661 *Research: Atmospheres* **102**:16391–16405.

662 Huang, H., L. D. Anderegg, T. E. Dawson, S. Mote, and P. D’Odorico. 2020. Crit-
663 ical transition to woody plant dominance through microclimate feedbacks in North
664 American coastal ecosystems. *Ecology* **101**:e03107.

665 Jongejans, E., K. Shea, O. Skarpaas, D. Kelly, and S. P. Ellner. 2011. Importance of
666 individual and environmental variation for invasive species spread: a spatial integral
667 projection model. *Ecology* **92**:86–97.

668 Katul, G., A. Porporato, R. Nathan, M. Siqueira, M. Soons, D. Poggi, H. Horn, and
669 S. A. Levin. 2005. Mechanistic analytical models for long-distance seed dispersal by
670 wind. *The American Naturalist* **166**:368–381.

- 671 Keitt, T. H., M. A. Lewis, and R. D. Holt. 2001. Allee effects, invasion pinning, and
672 species' borders. *The American Naturalist* **157**:203–216.
- 673 Kelleway, J. J., K. Cavanaugh, K. Rogers, I. C. Feller, E. Ens, C. Doughty, and N. Sain-
674 tilan. 2017. Review of the ecosystem service implications of mangrove encroachment
675 into salt marshes. *Global Change Biology* **23**:3967–3983.
- 676 Knapp, A. K., J. M. Briggs, S. L. Collins, S. R. Archer, M. S. BRET-HARTE, B. E.
677 Ewers, D. P. Peters, D. R. Young, G. R. Shaver, E. Pendall, et al. 2008. Shrub
678 encroachment in North American grasslands: shifts in growth form dominance rapidly
679 alters control of ecosystem carbon inputs. *Global Change Biology* **14**:615–623.
- 680 Kot, M., M. A. Lewis, and P. van den Driessche. 1996. Dispersal data and the spread of
681 invading organisms. *Ecology* **77**:2027–2042.
- 682 Lei, S. A. 1999. Ecological impacts of *Pogonomyrmex* on woody vegetation of a *Larrea*-
683 *Ambrosia* shrubland. *The Great Basin Naturalist* pages 281–284.
- 684 Lewis, M., and P. Kareiva. 1993. Allee dynamics and the spread of invading organisms.
685 *Theoretical Population Biology* **43**:141–158.
- 686 Mabry, T. J., J. H. Hunziker, D. Difeo Jr, et al. 1978. Creosote bush: biology and
687 chemistry of *Larrea* in New World deserts. Dowden, Hutchinson & Ross, Inc.
- 688 Maddox, J. C., and S. Carlquist. 1985. Wind dispersal in Californian desert plants:
689 experimental studies and conceptual considerations. *Aliso: A Journal of Systematic*
690 *and Evolutionary Botany* **11**:77–96.
- 691 Milne, B. T., D. I. Moore, J. L. Betancourt, J. A. Parks, T. W. Swetnam, R. R. Par-
692 menter, and W. T. Pockman. 2003. Multidecadal drought cycles in south-central New
693 Mexico: Patterns and consequences. Oxford University Press: New York, NY.

- 694 Moore, D., and K. Hall, 2022. Meteorology Data from the Sevilleta
695 National Wildlife Refuge, New Mexico. Environmental Data Initiative.
696 <https://doi.org/10.6073/pasta/d56307b398e28137dabaa6994f0f5f92>.
- 697 Moreno-de las Heras, M., L. Turnbull, and J. Wainwright. 2016. Seed-bank structure
698 and plant-recruitment conditions regulate the dynamics of a grassland-shrubland Chi-
699 huahuan ecotone. *Ecology* **97**:2303–2318.
- 700 Mugasi, S., E. Sabiiti, and B. Tayebwa. 2000. The economic implications of bush
701 encroachment on livestock farming in rangelands of Uganda. *African Journal of Range*
702 *and Forage Science* **17**:64–69.
- 703 Nathan, R., G. G. Katul, G. Bohrer, A. Kuparinen, M. B. Soons, S. E. Thompson,
704 A. Trakhtenbrot, and H. S. Horn. 2011. Mechanistic models of seed dispersal by wind.
705 *Theoretical Ecology* **4**:113–132.
- 706 Neubert, M. G., and H. Caswell. 2000. Demography and dispersal: calculation and
707 sensitivity analysis of invasion speed for structured populations. *Ecology* **81**:1613–
708 1628.
- 709 Oba, G., E. Post, P. Syvertsen, and N. Stenseth. 2000. Bush cover and range condition
710 assessments in relation to landscape and grazing in southern Ethiopia. *Landscape*
711 *ecology* **15**:535–546.
- 712 Pan, S., and G. Lin. 2012. Invasion traveling wave solutions of a competitive system
713 with dispersal. *Boundary Value Problems* **2012**:120.
- 714 Parizek, B., C. M. Rostagno, and R. Sottini. 2002. Soil erosion as affected by shrub
715 encroachment in northeastern Patagonia. *Rangeland Ecology & Management/Journal*
716 *of Range Management Archives* **55**:43–48.

- 717 Peters, D. P., and J. Yao. 2012. Long-term experimental loss of foundation species:
718 consequences for dynamics at ecotones across heterogeneous landscapes. *Ecosphere*
719 **3**:1–23.
- 720 Ratajczak, Z., J. B. Nippert, and S. L. Collins. 2012. Woody encroachment decreases
721 diversity across North American grasslands and savannas. *Ecology* **93**:697–703.
- 722 Raupach, M. 1994. Simplified expressions for vegetation roughness length and zero-
723 plane displacement as functions of canopy height and area index. *Boundary-Layer*
724 *Meteorology* **71**:211–216.
- 725 Ravi, S., P. D’Odorico, S. L. Collins, and T. E. Huxman. 2009. Can biological invasions
726 induce desertification? *The New Phytologist* **181**:512–515.
- 727 Reed, M., L. Stringer, A. Dougill, J. Perkins, J. Athlapheng, K. Mulale, and N. Favretto.
728 2015. Reorienting land degradation towards sustainable land management: Linking
729 sustainable livelihoods with ecosystem services in rangeland systems. *Journal of envi-*
730 *ronmental management* **151**:472–485.
- 731 Reynolds, J. F., R. A. Virginia, P. R. Kemp, A. G. De Soyza, and D. C. Tremmel. 1999.
732 Impact of drought on desert shrubs: effects of seasonality and degree of resource island
733 development. *Ecological Monographs* **69**:69–106.
- 734 Roques, K., T. O’connor, and A. R. Watkinson. 2001. Dynamics of shrub encroach-
735 ment in an African savanna: relative influences of fire, herbivory, rainfall and density
736 dependence. *Journal of Applied Ecology* **38**:268–280.
- 737 Schlesinger, W. H., and A. M. Pilmanis. 1998. Plant-soil interactions in deserts. *Biogeo-*
738 *chemistry* **42**:169–187.
- 739 Schlesinger, W. H., J. A. Raikes, A. E. Hartley, and A. F. Cross. 1996. On the spatial

740 pattern of soil nutrients in desert ecosystems: ecological archives E077-002. *Ecology*
741 **77**:364–374.

742 Schlesinger, W. H., J. F. Reynolds, G. L. Cunningham, L. F. Huenneke, W. M. Jarrell,
743 R. A. Virginia, and W. G. Whitford. 1990. Biological feedbacks in global desertification.
744 *Science* **247**:1043–1048.

745 Sirami, C., and A. Monadjem. 2012. Changes in bird communities in Swaziland savannas
746 between 1998 and 2008 owing to shrub encroachment. *Diversity and Distributions*
747 **18**:390–400.

748 Skarpaas, O., and K. Shea. 2007. Dispersal patterns, dispersal mechanisms, and invasion
749 wave speeds for invasive thistles. *The American Naturalist* **170**:421–430.

750 Sullivan, L. L., B. Li, T. E. Miller, M. G. Neubert, and A. K. Shaw. 2017. Density depen-
751 dence in demography and dispersal generates fluctuating invasion speeds. *Proceedings*
752 *of the National Academy of Sciences* **114**:5053–5058.

753 Taylor, C. M., and A. Hastings. 2005. Allee effects in biological invasions. *Ecology*
754 *Letters* **8**:895–908.

755 Thompson, S. E., S. Assouline, L. Chen, A. Trahtenbrot, T. Svoray, and G. G. Katul.
756 2014. Secondary dispersal driven by overland flow in drylands: Review and mechanistic
757 model development. *Movement ecology* **2**:7.

758 Trollope, W., F. Hobson, J. Danckwerts, and J. Van Niekerk. 1989. Encroachment and
759 control of undesirable plants. *Veld management in the Eastern Cape* pages 73–89.

760 Turnbull, L., J. Wainwright, and R. E. Brazier. 2010. Changes in hydrology and erosion
761 over a transition from grassland to shrubland. *Hydrological Processes: An Interna-*
762 *tional Journal* **24**:393–414.

- 763 Van Auken, O. 2009. Causes and consequences of woody plant encroachment into western
764 North American grasslands. *Journal of environmental management* **90**:2931–2942.
- 765 Van Auken, O. W. 2000. Shrub invasions of North American semiarid grasslands. *Annual*
766 *review of ecology and systematics* **31**:197–215.
- 767 Vasek, F. C. 1980. Creosote bush: Long-lived clones in the Mojave Desert. *American*
768 *Journal of Botany* **67**:246–255.
- 769 Veit, R. R., and M. A. Lewis. 1996. Dispersal, population growth, and the Allee ef-
770 fect: dynamics of the house finch invasion of eastern North America. *The American*
771 *Naturalist* **148**:255–274.
- 772 Wang, M.-H., M. Kot, and M. G. Neubert. 2002. Integrodifference equations, Allee
773 effects, and invasions. *Journal of mathematical biology* **44**:150–168.
- 774 Wells, P. V., and J. H. Hunziker. 1976. Origin of the creosote bush (*Larrea*) deserts of
775 southwestern North America. *Annals of the Missouri Botanical Garden* pages 843–861.
- 776 Whitford, W., E. Depree, and P. Johnson. 1980. Foraging ecology of two chihuahuan
777 desert ant species: *Novomessor cockerelli* and *Novomessor albigulosus*. *Insectes Sociaux*
778 **27**:148–156.
- 779 Whitford, W. G. 1978. Structure and seasonal activity of Chihuahua desert ant commu-
780 nities. *Insectes Sociaux* **25**:79–88.
- 781 Wiernga, J. 1993. Representative roughness parameters for homogeneous terrain.
782 *Boundary-Layer Meteorology* **63**:323–363.
- 783 Williams, J. L., T. E. Miller, and S. P. Ellner. 2012. Avoiding unintentional eviction
784 from integral projection models. *Ecology* **93**:2008–2014.
- 785 Wood, S. 2017. *Generalized Additive Models: An Introduction with R*. 2 edition.
786 Chapman and Hall/CRC.

787 Appendix A: Dispersal kernel modeling

788 **WALD dispersal kernel** In order to create the dispersal kernel, we first take the wind
 789 speeds at measurement height z_m and correct them to find wind speed U for any height
 790 H by using the logarithmic wind profile ⁵

$$791 \quad U = \frac{1}{H} \int_{d+z_0}^H \frac{u^*}{K} \log \left(\frac{z-d}{z_0} \right) dz \quad (10)$$

792 given in Bullock et al. (2012) equation 6, with the notation slightly modified. Here,
 793 z is the height above the ground, K is the von Karman constant, and u^* is the friction
 794 velocity. The zero-plane displacement d and roughness length z_0 are surface roughness
 795 parameters that, for a grass canopy height h above the ground, are approximated by
 796 $d \approx 0.7h$ and $z_0 \approx 0.1h$. These estimates are from Raupach (1994) for a canopy area
 797 index $\Lambda = 1$ in which the sum of grass canopy elements is equal to the unit area being
 798 measured. A 0.15 m grass height at our study site gives $d = 0.105$ and z_0 , which are
 799 suitable approximations for grassland (Wiernga, 1993). Calculations of u^* were done
 800 using equation A2 from Skarpaas and Shea (2007), in which

$$801 \quad u^* = KU_m \left[\log \left(\frac{z_m - d}{z_0} \right) \right]^{-1} \quad (11)$$

802 and U_m is the mean wind velocity at the measurement height z_m . Values for the
 803 turbulent flow parameter σ were then calculated using the estimate made by Skarpaas
 804 and Shea (2007) in their equation A4, where

$$805 \quad \sigma = 2A_w^2 \sqrt{\frac{K(z-d)u^*}{C_0U}} \quad (12)$$

806 and C_0 is the Kolmogorov constant. A_w is a constant that relates vertical turbulence
 807 to friction velocity and is approximately equal to 1.3 under the assumptions of above-

⁵ *We need to describe and cite the wind data used here.*

canopy flow made by Skarpaas and Shea (2007), based off calculations from Hsieh and Katul (1997). In addition, the assumption that $z = H$ was made in order to make the calculation of σ more feasible.⁶

The values from the previous three equations give us the necessary information to calculate μ' and λ' , thus allowing us to create the WALD distribution $p(r)$. However, the base WALD model does not take into account variation in wind speeds or seed terminal velocities, which limits its applicability in systems where such variation is present. In order to account for this variation, we integrate the WALD model over distributions of these two variables using the same method as Skarpaas and Shea (2007). Additionally, the WALD model assumes seed release from a single point source, which is not realistic for creosote bush; because seeds are released across the entire height of the shrub rather than from a point source, we integrated $p(r)$ across the uniform distribution from the grass canopy height to the shrub height. Thus, under the assumptions that the height at which a seed is located does not affect its probability of being released and that seeds are evenly distributed throughout the shrub, this gives the dispersal kernel $K(r)$, where

$$K(r) = \iiint p(F)p(U)p(z)p(r) dF dU dz \quad (13)$$

and $p(F)$ and $p(U)$ are the PDFs of the terminal velocity F and wind speed U , respectively, and $p(z)$ is the uniform distribution from h to H .

Dispersal data collection The distribution $p(F)$ in the integral above was constructed using experimentally determined seed terminal velocities. This was done by using laboratory-based seed release experiments with a high-speed camera and motion tracking software to determine position as a function of time. We then used the Levenberg-Marquardt algorithm to solve a quadratic-drag equation of motion for F . Before seeds were released, they were dried, dyed with yellow fluorescent powder, and then

⁶ *Can you describe this assumption in biological terms?*

832 put against a black background to improve visibility and make tracking easier. While the
833 powder added mass to the seeds, this added mass only yielded an approximately 2.5%
834 increase, likely having little effect on terminal velocities. Measurements were conducted
835 for 48 seeds that were randomly chosen from a seed pool derived from different plants,
836 and then an empirical PDF of terminal velocities was constructed using the data. Con-
837 structing $p(U)$ involved creating an empirical PDF of hourly wind speeds using data from
838 a Sevilleta LTER meteorological station (Five Points), the station closest to our transects.
839 We used wind speed data collected from 1988 to 2010.⁷

⁷ *Most SEV data sets have a doi, so ideally we should cite the wind speed data.*